Large Area Light-Pulse Atom Interferometry

J. M. McGuirk, M. J. Snadden, and M. A. Kasevich
Physics Department, Yale University, New Haven, Connecticut 06520
(Received 7 July 2000)

We report the experimental demonstration of a large area atom interferometer based on extended sequences of light pulses. We characterize the interferometer through measurement of the acceleration due to gravity and demonstrate a threefold enhancement in intrinsic acceleration sensitivity. The technique is applicable to many atom interferometer configurations, including those used for measurement of rotations, gravity gradients, and $\hbar/m$.

PACS numbers: 39.20.+q, 03.75.Dg, 04.80.–y, 32.80.Pj

Atom interferometers based on pulses of light have shown promise in many applications, both scientific and technical. For example, the sensitivity and accuracy of light-pulse atom interferometer gyroscopes [1,2], gravimeters [3], and gravity gradiometers [4,5] compare favorably with the performance of state-of-the-art instruments, while the light-pulse method is likely to lead to a more precise determination of $\hbar/m_{Cs}$ [6]. The light-pulse approach uses sequences of optical pulses to generate the atom optical elements (e.g., mirrors and beam splitters) for coherent manipulation of atomic wave packets [7,8]. In this Letter, we describe a general technique for increasing the sensitivity of a light-pulse atom interferometer using extended sequences of optical pulses. This technique does not sacrifice instrument accuracy or counting statistics and is likely to lead to significant performance gains for existing instruments. In the proof-of-concept work described below, we demonstrate a threefold enhancement in sensitivity for an atom interferometer accelerometer.

For the precision measurements identified above, measurement sensitivity is proportional to the relative momentum imparted to atomic wave packets by the beam splitting elements [9]. These past measurements used beam splitting techniques which imparted a relative momentum difference of $2\hbar k$ to interfering wave packets (k is the propagation vector of the laser used to manipulate the atomic wave packets). The new pulse sequences presented here offer a method of increasing the sensitivity of these devices by increasing the beam splitter momentum transfer. In particular, we report demonstration of an interferometer operating with $6\hbar k$ momentum transfer between wave packets. Our method is extendable to $(4N + 2)\hbar k$ (integer N).

Previous work using high-order Bragg processes has demonstrated interference with a momentum transfer of $6\hbar k$ [10]. High-order Bragg processes, however, place very tight constraints on the initial momentum spread of the atomic source along the axis of the Bragg beams. Meeting this constraint sacrifices atomic flux, thus sensitivity, through a reduction in counting statistics. Interferometers based on Raman-Nath standing-wave interactions can operate with a mean momentum transfer larger than $2\hbar k$ [11]. However, the Raman-Nath process inefficiently populates higher-lying momentum states, and interferometers based on this process have not been shown to operate at high statistical sensitivity. Adiabatic transfer has been used to transfer up to $100\hbar k$ to pairs of atomic wave packets [12]. In these experiments, however, the relative momentum between interfering wave packets was $2\hbar k$. In related work, adiabatic transfer was used to generate $4\sqrt{2}\,\hbar k$ momentum transfer [13] and $8\hbar k$ [14]. These schemes, however, are unsuitable for precision interferometry, as they require the use of atomic transitions which are first-order sensitive to the magnetic field. In the work described below, large momentum transfer is obtained without sacrificing count rates or introducing systematic offsets.

Before summarizing the principles underlying our technique, we first review the basic light-pulse method [7,15]. In this method, traveling-wave pulses of light resonantly couple two long-lived electronic states. First a beam splitting pulse puts the atom into a coherent superposition of its two internal states. Because of conservation of momentum during the atom-light interaction, this pulse introduces a relative momentum between the atomic wave packets in each state. These wave packets are allowed to drift apart for a time T, after which a mirror pulse is applied to redirect the two wave packets. After another interval of duration T, the wave packets physically overlap, and a final beam splitting pulse recombines them. This leads to path dependent interference in the probability amplitudes to detect the atom in a given internal state. In our work based on stimulated Raman transitions between ground state hyperfine levels, this momentum difference is $\hbar|\mathbf{k}_1 - \mathbf{k}_2| \approx 2\hbar k$, where $\mathbf{k}_1$ and $\mathbf{k}_2$ are the propagation vectors associated with each of the lasers used to drive the two-photon transition and $\mathbf{k}_1 \approx -\mathbf{k}_2$.

Our $6\hbar k$ interferometer sequence consists of three parts: an initial beam splitting pulse sequence, a mirror sequence, and a recombining sequence. This sequence, depicted in Fig. 1, is similar to the basic sequence described in the previous paragraph, except each individual pulse is now replaced with a sequence of light pulses. The initial beam splitter consists of two pulses of light that are spaced closely by time τ. The first is a Raman pulse of pulse

 0031-9007/00/85(21)/4498(4)$15.00

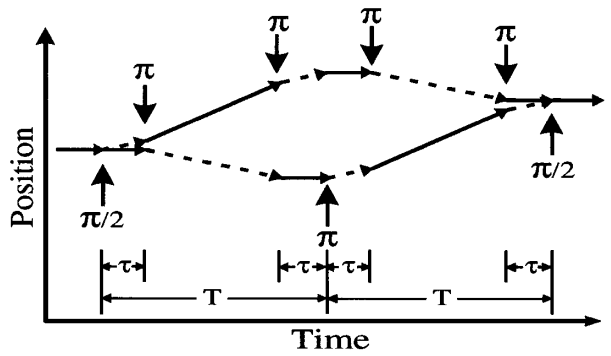

FIG. 1. Recoil diagram for the $6\hbar k$ interferometer. Dotted lines represent wave packets in the upper hyperfine ground state while solid lines depict the lower ground state. The Raman pulses are denoted by π and $\pi/2$ with an arrow in the propagation direction.

area $\pi/2$. Next, a π pulse is applied in rapid succession, but with the optical propagation vectors reversed. This π pulse further splits the atomic wave packets in momentum by increasing the momentum difference between wave packets to $6\hbar k$. The atoms are allowed to drift freely for a time $T - 2\tau$ that is usually long in comparison to both the pulse length and the time τ between the beam splitter pulses [see Fig. 2(a)]. A series of three π pulses in rapid succession, each of alternating propagation direction, acts as a mirror by redirecting the wave packets back towards each other with relative momentum $-6\hbar k$. After another free evolution period of time $T - 2\tau$ a final beam splitting sequence recombines the atomic wave packets. This sequence consists of a π pulse and then a final $\pi/2$ pulse with reversed propagation vectors. This method is related to earlier proposals which employ sequences of optical pulses to manipulate atomic wave packets [16]. The difference between these proposals and our experiments is that, in our experiments, pulse parameters are chosen to address both interferometer arms simultaneously, whereas in the previously proposed schemes, additional pulses address only one arm of the interferometer at a time.

In the absence of any external forces, atoms initially prepared in a particular state will return to that state with unit probability. However, the presence of a uniform external acceleration introduces a relative phase shift between the interfering paths. This phase shift modifies the internal state transition probabilities; hence measurement of the transition probability enables determination of the phase shift and ultimately measurement of the perturbing force.

There are two sources for this phase shift: the phase resulting from the atom's interaction with the laser light fields and the phase acquired during wave packet propagation in the intervals between the pulses [9,15]. If these contributions are evaluated with respect to the classical trajectories associated with the mean position of the atomic wave packets, the latter component vanishes. In the limit of short, intense pulses, the optical phase shift can be determined from the following rules which govern the evolution of the probability amplitude associated with each internal state: $|1\rangle \rightarrow e^{i\phi(t)}|2\rangle$ and $|2\rangle \rightarrow e^{-i\phi(t)}|1\rangle$, where $\phi(t)$ is the phase of the driving field at the mean position of the wave packet at the time of the pulse interaction, and states $|1\rangle$ and $|2\rangle$ are resonantly coupled by the stimulated Raman interaction.

We now calculate the acceleration induced phase shift for the $6\hbar k$ interferometer. Applying the rules outlined in the previous paragraph, we find $\Delta\phi = [\phi(t_1) + 2\phi(t_2)] - 2[\phi(t_3) + \phi(t_4) + \phi(t_5)] + [2\phi(t_6) + \phi(t_7)]$. The three quantities in square brackets correspond to the phase imparted to the atoms by the initial beam splitting pulses, the mirror pulses, and the recombining pulses. Here t_i is the time of the ith pulse, and $\phi(t_i) = (\mathbf{k}_1 - \mathbf{k}_2) \cdot \mathbf{x}(t_i) + \phi_i^0$ are the effective phases of the laser fields at the positions $\mathbf{x}(t_i)$. The positions $\mathbf{x}(t_i)$ are evaluated with respect to the classical trajectories associated with the atomic wave packets and ϕ_i^0 is the phase reference for the ith pulse [17]. This expression simplifies to $\Delta\phi = 3(\mathbf{k}_1 - \mathbf{k}_2) \cdot \mathbf{a}T^2 - 4(\mathbf{k}_1 - \mathbf{k}_2) \cdot \mathbf{a}T\tau + \phi^0$, where ϕ^0 is an overall phase factor (resulting from the initial phases ϕ_i^0). In our geometry, this becomes $\Delta\phi \simeq 6kaT^2 - 8kaT\tau + \phi^0$. This shift is approximately 3 times the phase shift expected from a $\pi/2 - \pi - \pi/2$ pulse sequence for long interrogation times T. The area enclosed by interfering wave packet trajectories has increased by the same factor [18]. The associated transition probability (our observable) is $P = [1 - \cos(\Delta\phi)]/2$.

The apparatus used in the $6\hbar k$ interferometer has been described in detail elsewhere and will be summarized here [4]. An ensemble of Cs atoms is prepared in a magneto-optical trap and launched in an atomic fountain, where it interacts with the Raman beams. The two Raman beams counterpropagate vertically through the chamber. Each experiment cycle lasts 750 ms and has three parts: ensemble preparation, interrogation, and detection. Each part will be briefly discussed below.

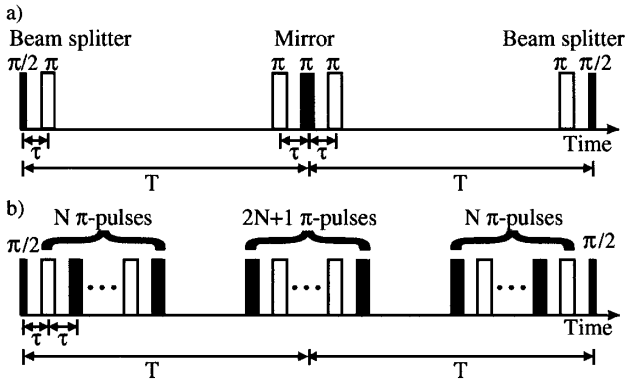

FIG. 2. Time domain representation of the interferometer. Light and dark pulses represent Raman pulses of opposite propagation direction. (a) is the $6\hbar k$ interferometer, while (b) shows a $(4N + 2)\hbar k$ interferometer.

The Cs atoms are loaded in the magneto-optical trap from a vapor cell and cooled to 2 μK. The atoms are then launched in a 12 cm high atomic fountain. The launch is performed by differentially detuning the molasses beams to create a moving optical molasses. Immediately after launching, the atoms undergo a state selection sequence designed to leave only a cold sample of atoms in the $6S_{1/2}$ $F = 3$, $m_f = 0$ ground state.

This state selection is performed as follows. Atoms are initially optically pumped into the $6S_{1/2}$ $F = 4$ ground state. A small bias field of about 30 mG separates the magnetic sublevels, and a rf pulse transfers atoms from the $F = 4$, $m_f = 0$ level to the $F = 3$, $m_f = 0$ level. A resonant, traveling-wave pulse of light clears away the unselected atoms in the $F = 4$ states. Another rf pulse transfers the remaining atoms to the $F = 4$, $m_f = 0$ state, and then a velocity selective Raman pulse returns colder atoms back into the $F = 3$, $m_f = 0$ state. A final resonant traveling-wave pulse removes the hotter atoms left in the $F = 4$ state.

Next the sequence of Raman pulses is applied. The two Raman lasers are generated by first passing an 852 nm master diode laser twice through a 4.6 GHz acousto-optic modulator (AOM). The up-shifted and down-shifted diffracted orders injection lock two 150 mW diode lasers [19]. The AOM is driven by a stable oscillator which sets the frequency difference of the two lasers to the hyperfine ground state splitting of Cs. The two beams are combined with orthogonal polarizations on a polarizing beam splitting cube, pass through a Pockels cell polarization modulator, and are spatially filtered with a pinhole. The modulator is used to reverse the beams' propagation directions, as described below. The two Raman beams copropagate to a polarizing beam splitting cube assembly above the chamber [4]. There they are split so that one beam propagates directly down through the atom cloud while the other beam propagates off the central axis of the chamber parallel to the axial beam. A pair of mirrors below the chamber redirects the off-axis beam to propagate upward along the axis of the chamber, giving two counterpropagating axial beams. After the beam splitting cubes, each Raman beam passes through a quarter-wave plate in order to give both beams σ^+ polarization. An HP8770A arbitrary wave form generator drives two low frequency AOMs that act as switches for the Raman beams and control their phases. The Raman π pulses are typically 30 μs long, and each Raman laser is detuned about 2 GHz from the $6P_{3/2}$, $F = 5$ level.

The Raman propagation vector reversal is achieved by means of the Pockels cell. Adjusting the voltage applied to the Pockels cell simultaneously rotates the polarization of the orthogonally polarized Raman beams. Rotating the polarization of each beam by 90° changes the direction each beam takes through the vacuum chamber, resulting in a reversal of the propagation vector for the Raman transitions. The Pockels cell nominally can switch polarizations in $\sim$1 μs but takes about 150 μs to settle completely. For this reason, $\tau = 150$ μs is the minimum time we use between pulses in the pulse sequence.

After the interrogation sequence, a blue detuned light pulse removes the atoms in the $F = 4$, $m_f = 0$ level, leaving the atoms in the $F = 3$, $m_f = 0$ state to be detected. During the fountain, the atom cloud ballistically expands to around $\sim$1 cm diameter. In order to detect the atoms with a high signal-to-noise ratio, an off-resonant magneto-optical trap is flashed on for 15 ms in order to compress the remaining atoms to $\sim$2 mm. After compression, two counterpropagating, resonant detection beams are turned on, and a photomultiplier tube detects fluorescence resulting from these beams.

We obtain interference fringes by electronically scanning the phase of the middle interferometer pulse [20]. The phase of each fringe is found by performing a least squares fit on each 50 point interference scan. By varying the free evolution time in the interferometer, we obtain a curve of phase shift versus expansion time T (see Fig. 3). Each point is an average of 20 interference scans. We compare the gravitational phase shift from $2\hbar k$ and $6\hbar k$ interferometers. The solid lines represent theoretical fits to the data of $\Delta\phi = 2kgT^2$ for the $2\hbar k$ interferometer and $\Delta\phi = 6kgT^2 - 8kgT\tau$ for the $6\hbar k$ interferometer. The only free parameter is a constant phase offset which results from the initial arbitrary phases ϕ_i^0.

Using the $6\hbar k$ interferometer we have extended the interferometer time T to 30 ms (Fig. 4). For $T > 30$ ms, the fringes are obscured by excessive phase noise from vibrations of the Raman retroreflecting mirrors below the chamber. To move to longer times, the mirror assembly must be placed on a vibrationally isolated platform to preserve fringes. A differential measurement of two ensembles of

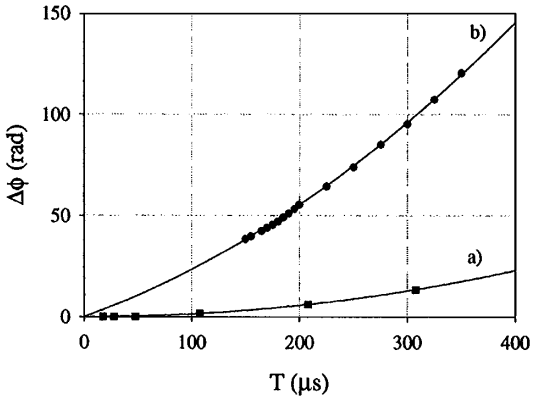

FIG. 3. Comparison of phase shift $\Delta\phi$ due to gravity as a function of free expansion time T for (a) $2\hbar k$ and (b) $6\hbar k$ interferometers. Solid lines are theoretical curves. Each interferometer had an arbitrary constant phase offset due to particular pulse parameters that has been suppressed. The phase uncertainty for each point is about ± 15 mrad, giving excellent agreement with theory.

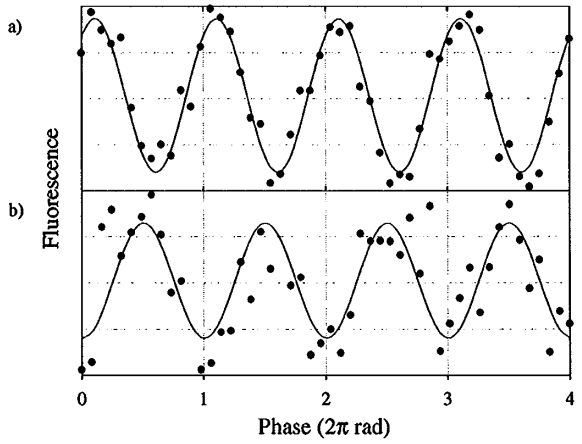

FIG. 4. Sample interference fringes from (a) $2\hbar k$ and (b) $6\hbar k$ interferometers taken with $T = 30$ ms. Each scan is acquired in 38 s. Typical fringe contrast is 40% and 25%, respectively. Solid lines are least squares fits. The extra noise in the $6\hbar k$ case is due to increased sensitivity to vibrations.

atoms performed using the same beams allows vibrational phase noise to be removed in a common mode way [4].

In principle, this process is extendable up to $(4N + 2)\hbar k$ momentum transfer by adding extra π pulses, as illustrated in Fig. 2(b). The essential idea is that application of subsequent pulses with reversed propagation vectors leads to a linear accumulation of the optical phase in the atomic coherences. This leverages interferometer sensitivity by providing a finer grained ruler for determining force-induced changes in wave packet positions.

In practice, several factors limit the length of the pulse sequence which may be used. First, spontaneous emission due to weak coupling to the allowed single-photon optical transitions homogeneously dephases the atomic coherence and places a lower limit on the optical detuning for the Raman pulses [21]. This places an upper limit on the two-photon Rabi frequency. For our parameters, we experience 1% spontaneous emission for each π pulse. Second, the Gaussian spatial profile of the Raman beams leads to an inhomogeneous distribution of effective Rabi frequencies. This introduces a spread in pulse area across the atomic spatial distribution and ultimately limits the ensemble transfer efficiency of each π pulse. Finally, the frequency selectivity of the interrogating pulses limits the number of pulses in the sequence, as the linewidth of each pulse needs to accommodate the differential Doppler shifts in the transition frequencies due to the recoil momentum imparted to the atomic wave packets by previous pulses.

We are exploring methods to overcome the above limitations to realize high momentum transfer atom optics. We believe that there are no serious barriers to realization of momentum transfers greater than $10\hbar k$. Such high momentum beam splitters would offer new levels of sensitivity for atom interferometer based precision measurements.

This work was supported by the ONR and NASA.

[1] T. L. Gustavson, P. Bouyer, and M. A. Kasevich, Phys. Rev. Lett. **78**, 2046 (1997).
[2] T. L. Gustavson, A. Landragin, and M. A. Kasevich, Classical and Quantum Gravity **17**, 2385 (2000).
[3] A. Peters, C. Keng Yeow, and S. Chu, Nature (London) **400**, 849 (1999).
[4] M. J. Snadden *et al.,* Phys. Rev. Lett. **81**, 971 (1998).
[5] D. Durfee *et al.,* in *Proceedings of the IEEE 2000 Position, Location, and Navigation Symposium, San Diego, CA, 2000* (IEEE, Piscataway, NJ, 2000), Vol. 535, p. 395.
[6] D. S. Weiss, B. C. Young, and S. Chu, Phys. Rev. Lett. **70**, 2706 (1993); Appl. Phys. B **59**, 217 (1994).
[7] C. J. Bordé, Phys. Lett. A **140**, 10 (1989).
[8] M. Kasevich and S. Chu, Phys. Rev. Lett. **67**, 181 (1991); F. Riehle *et al.,* Phys. Rev. Lett. **67**, 177 (1991).
[9] *Atom Interferometry,* edited by P. Berman (Academic Press, New York, 1997).
[10] D. M. Giltner, R. W. McGowan, and S. A. Lee, Phys. Rev. Lett. **75**, 2638 (1995).
[11] S. B. Cahn *et al.,* Phys. Rev. Lett. **79**, 784 (1997).
[12] M. Weitz, B. C. Young, and S. Chu, Phys. Rev. Lett. **73**, 2563 (1994).
[13] P. D. Featonby *et al.,* Phys. Rev. Lett. **81**, 495 (1998).
[14] M. Weitz, T. Heupel, and T. W. Hansch, Phys. Rev. Lett. **77**, 2356 (1996).
[15] M. Kasevich and S. Chu, Appl. Phys. B **54**, 321 (1992).
[16] See pp. 281–282 and 379–381 in Ref. [9].
[17] In our apparatus the phase is referenced to a mirror assembly below the atom ensemble off of which one of the Raman beams is reflected. This mirror is the origin for the atom's position vector $\mathbf{x}(t_i)$.
[18] We refer to the area enclosed in a recoil diagram (as illustrated in Fig. 1).
[19] P. Bouyer *et al.,* Opt. Lett. **21**, 1502 (1996).
[20] We scan the phase by electronically shifting the phase of the rf signal source used to drive the low frequency AOMs in the Raman pulse generation subsystem.
[21] The two-photon Rabi frequency scales as Ω^2/Δ, where Ω is the single-photon Rabi frequency and Δ is the detuning from the optical resonance. See K. Moler *et al.,* Phys. Rev. A **45**, 342 (1992).